Chapter 5:
Surface-atmosphere Exchange Parameters from
Aircraft and Ground-based Observations

Chapter Contents

5.1 Introduction

5.1.1 General

The exchanges of momentum, heat, water and carbon at the Earth's surface are the fundamental mechanisms by which the atmosphere, biosphere and hydrosphere are linked. These linkages span a wide range of spatial and temporal scales, from individual leaves to continents and from seconds to decades, and play a critical role in determining the response of the biosphere to, and modulation of, the climate. The range of scales makes it attractive to find quantities that describe and predict these exchanges over a range of space and time scales. Such quantities are called surface-atmosphere exchange parameters and may describe purely mechanical processes, for example, flow over aerodynamically rough bodies or purely physiological processes such as the response of stomata to meteorological conditions.

Here, the discussion is narrowed to the surface-atmosphere exchange of water vapour, through evaporation and transpiration, and the exchange of carbon dioxide through assimilation and respiration. Momentum is not explicitly considered and sensible heat is only considered as the residual in the surface energy budget. For ease of use, this subset of surface-atmosphere exchange parameters will be given the less cumbersome name of "surface properties". The investigation of surface properties is motivated by the realisation that the surface fluxes are determined by both the surface properties and the meteorology and that much of the temporal dependence in the fluxes arises from the meteorological forcing. The clearest examples of these are the diurnal variation in the fluxes and the variation in response to changing synoptic conditions. For the vegetated surfaces considered here, seasonal and longer time scales are likely to encompass significant changes in plant functionality and this will influence any surface properties describing the movement of water and carbon through these communities. The current investigation, however, is restricted to diurnal and synoptic time scales.

Regional estimates of surface properties are desirable for several reasons. First, their independence from meteorological conditions means that they reveal more information about surface heterogeneity than the surface fluxes and as a result may

be more easily related to remotely sensed quantities. Second, the independence from meteorology means they offer a convenient method for linking measurements at different time and space scales and from different platforms, for example from ground-based and airborne instruments. Third, they provide a means for estimating some of the regionally averaged parameters required by the soil-vegetation-atmosphere transport (SVAT) models that are now being incorporated into general circulation models (GCM) and provide a means to constrain or validate these models.

The most common platforms for estimating surface properties are ground-based flux stations and instrumented aircraft but the data from these have contrasting characteristics. Flux stations provide good temporal, but poor spatial resolution. This is because the source-area at the surface, typically $< 1 \, \text{km}^2$ (Horst and Weil, 1992), may not be representative of the larger region. Even when a large number of sites are used, bias in their location may lead to bias in estimates of surface heterogeneity and regional fluxes (Kelly et al. 1992). In contrast, aircraft can cover areas of the order of $100 \, \text{km}^2$ on time scales that are short compared to the diurnal cycle. They provide information on the spatial variability of the fluxes, but this carries a penalty of under-sampling in time at any given location. This temporal under-sampling can be mitigated by repeated flights over the same area to reduce the random error associated with the measurement and enhance the atmospheric signature from the underlying surface (Mahrt, 1998). However, the time taken to cover large areas means that repeated passes often take place on different days, under different meteorological conditions, and this complicates the analysis. The above points can be summarised as follows: towers provide good temporal but poor spatial resolution, whereas aircraft provide good spatial but poor temporal resolution. These complementary strengths make it attractive to find ways of combining tower and aircraft data so as to utilise the best features of both.

The same discussion can be extended to satellite observations. These share many of the spatial and temporal characteristics of aircraft data. Satellites provide excellent spatial coverage but sporadic temporal coverage due to orbital constraints and the need for cloud free conditions. This mimics the spatial and temporal coverage of aircraft data but satellites are not able to directly measure the turbulent fluxes. This

sharpens the search for appropriate surface properties that are independent of meteorological conditions, that can be derived from remotely sensed quantities and that can be used to calculate the fluxes. Many of the discussions in the following sections, particularly those concerning the links between aircraft and ground-based data, also apply to satellite data.

To combine successfully aircraft and tower measurements, some property of the surface is sought which has the following characteristics. First, it must vary across the surface in response to heterogeneity since ground-based observations lack spatial information and, if it is to be useful at all, the surface property must contain this missing information. Second, at any location, the surface property should remain constant throughout the day or its variation should be predictable using routine meteorological data from ground-based sites. This allows observations at a particular time of day, say from an aircraft or satellite, to be used for the whole day. Third, it must have a limited variation over time scales of a few days, that is to say, it should be insensitive to changes in synoptic conditions so that values determined on one day can be extrapolated to the next observation. This constraint can be relaxed to allow the surface property to vary as soil moisture levels change in response to loss via evapotranspiration or recharge via precipitation. These processes occur on time scales of several days or with intervals of several days and are likely to be resolved by infrequent aircraft or satellite passes. Finally, the surface property should be directly related to the surface fluxes, either by definition or via a mechanistic model.

This chapter examines two examples of such surface properties and assesses the extent to which they fulfil the above criteria. The first example is a collection of simple ratios formed from the surface fluxes: the evaporative fraction $\alpha_E = F_E/F_A$ (Mahrt, 1998), the Bowen ratio $\beta = F_H/F_E$ (Thom, 1975) and the water-use efficiency $W_{UE} = \lambda F_C/F_E$ (Tanner and Sinclair, 1983). The second example is a measure of the stomatal conductance, in this case the maximum stomatal conductance, g_{sx}, achievable by the vegetation under optimal meteorological conditions (Kelliher et al., 1995). This quantity is calculated by combining the Penman-Monteith equation for transpiration, an estimate of soil evaporation and a

simple model of stomatal response to light and humidity. The two approaches represent different degrees of sophistication, with α_E, β and W_{UE} being the simplest and g_{sx} being the more complicated.

The rationale for choosing the simple ratios is that they are easy to determine from ground-based and aircraft measurements and, in the case of α_E at least, its value at any given location appears to show little diurnal variation (Mahrt, 1998). The choice of g_{sx} comes from considering the factors that control the surface fluxes, in particular F_E. Atmospheric demand for water from the surface depends on the available energy (F_A), specific humidity saturation deficit (D), and aerodynamic conductance (G_a), while the ability of vegetation and soil to supply water to the atmosphere is described by the surface conductance (G_s). These factors are combined in the Penman-Monteith equation (Monteith, 1964). With the assumption that soil evaporation occurs at the equilibrium rate, Kelliher et al. (1995) developed a simple model for G_s in terms of leaf area index (L_{ai}), and leaf stomatal conductance (g_s). The latter varies diurnally in response to solar irradiance ($S_\downarrow$) and saturation deficit, and is bounded by g_{sx}, the maximum stomatal conductance of leaves at the top of the canopy. A key assumption in the current work is that g_{sx} is constant for each location for any given day, although it may vary with soil moisture content from day to day. Other models of stomatal function are available (Wang and Leuning, 1998) but these are more complex and require a greater number of ancillary parameters to be specified. The g_{sx} model is chosen in an attempt to introduce the most important mechanisms for a modest increase in complexity.

The remaining two sub-sections of this Introduction discuss some general aspects of the averaging of surface properties and the definitions and notation used in subsequent sections. The simple ratios, α_E, β and W_{UE} are then discussed (Section 5.2) followed by the maximum stomatal conductance model (Section 5.3). Results of both methods are presented in Section 5.4 and conclusions follow in Section 5.5.

5.1.2 Considerations For Averaging Surface Properties

Estimates of α_E, β, W_{UE} and g_{sx} from a single aircraft pass or a single ground-based observation may not be representative of the underlying surface due to random errors in the measurements. These may occur for a number of reasons such as cloud shadows, mesoscale events and incomplete resolution of long wavelength features (Mahrt, 1998). The error in a single measurement may even be sufficient to obscure the underlying surface heterogeneity. Averaging the data over several days, in the case of aircraft data, or over several averaging periods in the case of ground-based data, can reduce the random error in estimates of α_E, β, W_{UE} and g_{sx}.

The averaging of surface properties has been the subject of several papers over the last decade (Raupach, 1991; Lhomme, 1992; McNaughton, 1994; Raupach, 1995). In all of these treatments, the averaging of surface properties has been considered in the context of scale transitions, for example leaf to canopy or canopy to region. These investigations have generally been motivated by a desire to find averaging schemes that yield the correct final quantity, typically F_E, and preserve the form of some underlying model, typically the Penman-Monteith equation.

In the above studies, the case examined has always been that of averaging over a heterogeneous surface (leaf, canopy or region) at a single time, that is to say, spatial or areal averaging. The focus here is different, since the goal is to average over the same surface at multiple times, or temporal averaging. However, the techniques developed for spatial averaging can, if correctly formulated, be applied to the temporal averaging case with the following justifications.

Raupach (1995) formalises two generic constraints for the areal averaging of surface properties. The first is imposed by scalar conservation and Raupach (1995) demonstrates that this can only be satisfied when scalar fluxes are averaged linearly. This does not change when the averaging changes from spatial to temporal. The second constraint is imposed by the wish to preserve the form of the underlying model used to estimate the evaporation of water from a surface, in this case the Penman-Monteith equation. This constraint is, compared to the first, arbitrary since it is not prescribed by the physics of the situation. However, it does satisfy the

"conservation of complexity" (Raupach and Finnigan, 1995) principle and allows links to be drawn between surface properties at one scale and their counterparts at another, usually larger, scale. Again, this principle does not change when the averaging changes from spatial to temporal. This constraint, in combination with the first, is used to derive an averaging scheme for g_{sx} in Section 5.3.3.

5.1.3   Definitions and Notation

Aircraft data are collected over flight legs that are 10's to 100's of kilometres in length and represent spatial averages. Tower data are collected over periods from days to years and represent temporal averages. However, both have components of the other, for example aircraft flights take a finite time and a distinct upwind surface area influences the tower data. This section describes the spatial and temporal averaging inherent in aircraft and tower data, the different ways in which these are treated and the notation used in this thesis.

Tower data are taken as point measurements averaged over 30 minutes, and available throughout the day. Aircraft data provide an average along a line, either a 10 km segment of the transect or, by averaging data from the 6 grid legs, the 10 km by 8 km area covered by the grid pattern. To simplify matters, the 45 minutes taken by the aircraft to complete a transect or grid flight pattern is ignored and the aircraft data are treated as though they were spatial averages only. An additional complication arises because the aircraft data set consists of repeated passes over the same area at different times on several days. Combining aircraft data from several days with differing meteorological conditions (compositing) is a necessary and important part of the work presented here.

Angular brackets, $\langle \ \rangle$, are used to denote a spatial average. The subscripts i, j and k are used to identify the day, the time and the location at which an aircraft or ground based measurement was made. Capital letters I, J and K denote the number of days in the data set, the number of measurements used to form the daily average and the number of locations used to form the spatial average respectively.

5.2 Simple Ratios

5.2.1 Evaporative Fraction, Bowen Ratio and Water-use Efficiency

The spatially-averaged evaporative fraction for a particular location k, time of day j and day i is:

$$\langle \alpha_E \rangle_{ijk} = \frac{\langle F_E \rangle_{ijk}}{\langle F_A \rangle_{ijk}} .$$

$$5.1$$

$\langle F_E \rangle$ is the latent heat flux and $\langle F_A \rangle = \langle F_N \rangle - \langle F_G \rangle$ is the available energy. The spatial averages of F_E and F_A may be available from a ground-based network or from aircraft observations. The time-of-day dependence in Equation 5.1 can be eliminated by assuming that the diurnal trend in α_E can be neglected in which case $\langle \alpha_E \rangle_{ik} = \langle \alpha_E \rangle_{ijk}$. This allows the spatially-averaged evaporative fraction for a given location and day to be estimated from infrequent aircraft passes at different times of the day. Evidence to support the assumption is presented later in this chapter.

Two other simple ratios can be constructed from the fluxes of heat, water vapour and carbon dioxide. These are the Bowen ratio, β, and the water-use efficiency, W_{UE}, defined as follows:

$$\langle \beta \rangle_{ijk} = \frac{\langle F_H \rangle_{ijk}}{\langle F_E \rangle_{ijk}} ,$$

$$5.2$$

$$\langle W_{UE} \rangle_{ijk} = \frac{\lambda \langle F_C \rangle_{ijk}}{\langle F_E \rangle_{ijk}} .$$

$$5.3$$

$\langle F_H \rangle$ and $\langle F_C \rangle$ are the spatially-average fluxes of sensible heat and CO_2 respectively and λ is the latent heat of vapourisation. Note that W_{UE} as expressed here differs from the usual definition because F_E and F_C contain contributions from the canopy and the soil and the ratio of these contributions will change as L_{ai} and the

fraction of vegetation cover changes. This means that W_{UE} will vary across the landscape in response to both vegetation state and cover.

As with the evaporative fraction, β and W_{UE} are expected to show less diurnal variation than the fluxes themselves, in which case daily values can be estimated from infrequent aircraft flights. The diurnal and day-to-day variations of these quantities are examined in Sections 5.4.4 and 5.4.5 respectively. The estimation of regional-scale fluxes by combining the spatially-averaged ratios $\langle \alpha_E \rangle$, $\langle \beta \rangle$ and $\langle W_{UE} \rangle$ with ground-based measurements of the available energy is described in Chapter Seven.

5.2.2   Averaging Rules for Simple Ratios

Averaged values of α_E, β and W_{UE} were obtained by averaging the fluxes and then forming the ratios:

$$\langle \alpha_E \rangle_k = I^{-1} \left(\sum_{i=1}^{I} \langle F_E \rangle_{ik} \middle/ \sum_{i=1}^{I} \langle F_A \rangle_{ik} \right)$$

$$\langle \beta \rangle_k = I^{-1} \left(\sum_{i=1}^{I} \langle F_H \rangle_{ik} \middle/ \sum_{i=1}^{I} \langle F_E \rangle_{ik} \right) .$$

$$\langle W_{UE} \rangle_k = \lambda I^{-1} \left(\sum_{i=1}^{I} \langle F_C \rangle_{ik} \middle/ \sum_{i=1}^{I} \langle F_E \rangle_{ik} \right)$$

5.4

The random error in the resulting values of α_E, β and W_{UE} is reduced by the averaging process. However, the averaging also masks day-to-day variations in these quantities in response to changes in soil moisture.

5.3 Maximum Stomatal Conductance

5.3.1 Maximum Stomatal Conductance Model

Kelliher et al. (1995) showed that the surface conductance, G_s, could be written in terms of the canopy conductance (G_c), which in turn depends on leaf area index and the maximum stomatal conductance of leaves at the top of the canopy, g_{sx}. As with the simple ratios discussed above, it is assumed that there is no diurnal trend in g_{sx} so that it can be evaluated from aircraft measurements made at irregular times during the day. The diurnal and day-to-day variations in g_{sx} are examined in Sections 5.4.4 and 5.4.5. The estimation of regional-scale F_E by combining the spatially-averaged g_{sx} with ground-based measurements is described in Chapter Seven.

The key step in estimating g_{sx} is to solve the Penman-Monteith equation for G_s using measurements of F_A, F_E, D, and G_a. Canopy conductance is then estimated from G_s by assuming that soil evaporation occurs at the equilibrium rate, and g_{sx} is calculated from G_c by inverting a simple model of canopy conductance (Isaac et al, 2004b). The four equations on which the method is based are given below in their general forms before continuing with the actual equations used in order to emphasise the role of the spatially-averaged data.

Thom (1975) showed that the Penman-Monteith equation can be written as:

$$F_E = F_A \left(\frac{\varepsilon + G_a/G_i}{\varepsilon + 1 + G_a/G_s} \right) \qquad 5.5$$

where $G_i = F_A/(\rho \lambda D)$ is the isothermal conductance, in which ρ is the density of moist air, λ is the latent heat of vaporisation and ε is the change in latent heat content of saturated air with change in sensible heat content.

The aerodynamic conductance is estimated using:

$$G_a = \frac{ku_*}{\ln\left(\dfrac{z-d}{z_{0h}}\right) - \Psi\left(\dfrac{z-d}{L}\right) + \Psi\left(\dfrac{z_{0h}}{L}\right)}$$

$\qquad\qquad$ 5.6

where $z_{0h} = z_0/5$ (Thom, 1975) is the roughness length for heat, k is the von Karman constant, u_* is the friction velocity, z is the measurement height, d is the zero-plane displacement, L is the Monin-Obukov length and Ψ is a stability function (see Garratt (1992) for functional forms). The aerodynamic conductance for water vapour is assumed to equal that for heat. There is evidence that these quantities may differ (Lange et. al., 1983) but no reliable method exists to parameterise these differences. Equation 5.6 is only valid in the surface layer, in particular when $z/L \leq -1$. Above this height, u_* is no longer the appropriate velocity scale and the stability function $\Psi\left((z-d)/L\right)$ is no longer valid. Strictly speaking, the requirement for the aircraft height to satisfy $z/L \leq -1$ limits the method to low altitudes and moderately unstable conditions. However, Leuning et al. (2004) find that $G_a \approx 5G_s$ for the 1995 OASIS data, and point out that this reduces the influence of errors in G_a on the estimation of G_s.

Next, a relationship is developed between G_s and canopy conductance, G_c, and then an expression for G_c in terms of g_{sx} is introduced. When soil evaporation occurs at the equilibrium rate, Kelliher et al. (1995) showed that:

$$G_s = G_c\left(\frac{1 + G_a/(\varepsilon G_i) + \tau G_a/\left[(\varepsilon+1)G_c\right]}{1 + G_a/(\varepsilon G_i) - \tau}\right)$$

$\qquad\qquad$ 5.7

where $\tau = \exp\left(-c_A L_{ai}\right)$ is the fraction of available energy at the soil surface and c_A is an extinction coefficient.

Kelliher et al. (1995) also proposed a simple model relating G_c to absorbed solar irradiance ($S_\downarrow$), leaf area index (L_{ai}) and g_{sx}. This model has been modified here to include a term for the dependence of stomatal conductance on the saturation deficit, D, namely:

$$G_c = \frac{g_{sx}}{c_Q} \ln\left(\frac{S_\downarrow + S_{50}}{S_\downarrow \exp(-c_Q L_{ai}) + S_{50}}\right)\left(\frac{1}{1 + D/D_0}\right)$$

5.8

where $S_\downarrow$ is the solar irradiance, D is the saturation deficit and c_Q is the shortwave radiation extinction coefficient. (A value of 0.6 has been used for both c_Q and c_A; Denmead, 1976). S_{50} and D_0 are empirical constants in rectangular hyperbolae which describe the light and humidity responses of stomatal conductance. Equations 5.7 and 5.8 provide the relationship between surface conductance and maximum stomatal conductance. The equations used are presented in the remainder of this section with the averaging of the data made explicit.

The first step in estimating g_{sx} using this method is to invert the Penman-Monteith equation to get an expression for the spatially averaged surface conductance for a particular location k, time of day j and day i:

$$\langle G_s \rangle_{ijk} = \frac{\langle G_a \rangle_{ijk}}{\left(\langle F_A \rangle_{ijk} / \langle F_E \rangle_{ijk}\right)\left(\varepsilon + \langle G_a \rangle_{ijk} / \langle G_i \rangle_{ijk}\right) - (\varepsilon + 1)}$$

5.9

where $\langle G_a \rangle_{ijk}$ is estimated using Equation 5.6. Use of Equation 5.6 requires a value of z_{0h} to be specified for the averaging area and this may not be a simple average of the patch scale z_{0h} (Hasager and Jensen, 1999). However, G_a is relatively insensitive to z_{0h}. A factor of two variation in z_{0h} only results in a 15% change in G_a and errors from this source will be small.

The spatially-averaged canopy conductance is given by inversion of Equation 5.7:

$$\langle G_c \rangle_{ijk} = \frac{\langle G_s \rangle_{ijk}\left(1 + \langle G_a \rangle_{ijk} / \varepsilon \langle G_i \rangle_{ijk} - \tau\right) - \tau \langle G_a \rangle_{ijk} / (\varepsilon + 1)}{1 + \langle G_a \rangle_{ijk} / \varepsilon \langle G_i \rangle_{ijk}}.$$

5.10

The spatially averaged maximum stomatal conductance is then obtained by inverting Equation 5.8:

$$\langle g_{sx} \rangle_{ijk} = \frac{c_Q \langle G_c \rangle_{ijk} \left(1 + \langle D \rangle_{ijk} / D_0 \right)}{\ln \left(\dfrac{\langle S_\downarrow \rangle_{ijk} + S_{50}}{\langle S_\downarrow \rangle_{ijk} \exp\left(-c_Q L_{ai}\right) + S_{50}} \right)} . \qquad \text{5.11}$$

The maximum stomatal conductance is expected to be independent of the time of day and this leads to $\langle g_{sx} \rangle_{ik} = \langle g_{sx} \rangle_{ijk}$. However, g_{sx} may vary from day to day because of changes in the canopy conductance induced by changes in soil moisture. The omission of soil moisture in Equation 5.11 means that $\langle g_{sx} \rangle_{ijk}$ will be smaller than the values in Kelliher et al. (1995) and will vary across the landscape in response to variations in soil moisture if the vegetation is water stressed.

5.3.2   Determination of Model Parameters

The values of g_{sx}, S_{50} and D_0 must be specified before the model for surface conductance given in Equations 5.7 and 5.8 can be used.

Empirical constants in models are often chosen to minimise some measure of the residual between the model predictions and the observations. The measure used here was the root mean square difference between the observed and modelled values of canopy conductance normalised by the average observed value. This quantity is denoted by Ω and is defined as:

$$\Omega = N^{-1} \sum_{n=1}^{N} RMS_n / \overline{G}_{c,n}^{obs}$$

$$RMS_n = \sqrt{ I_n^{-1} \sum_{i=1}^{I_n} \left(G_{c,n,i}^{obs} - G_{c,n,i}^{mod} \right)^2 } \qquad \text{5.12}$$

where G_c^{obs} is the observed canopy conductance, G_c^{mod} is the modelled canopy conductance, N is the number of sites, I_n is the number of observations at site n, $\overline{G}_{c,n}^{obs} = I^{-1} \sum_i G_{c,n,i}^{obs}$ is the mean observed canopy conductance at site n and the subscripts i and n refer to individual observations and sites respectively.

The term $\left(G_{c,n,i}^{obs} - G_{c,n,i}^{mod}\right)^2$ in Equation 5.12 makes RMS_n sensitive to outlying G_c^{obs} points. These may occur for several reasons including random and systematic errors in the fluxes, non-closure of the surface energy budget and direct evaporation of water from the canopy, for example, after dewfall or rain. Outlying points were defined as those where the ratio of the turbulent fluxes to the available energy fell outside the range $0.75 \leq \left(F_H + F_E\right)/\left(F_N - F_G\right) \leq 1.25$ and where anomalously high values of G_c^{obs} occurred before 1100 on days when D dropped to ≤ 0.05 kg kg^{-1} overnight. These points were identified by manual inspection and removed from the data set used to determine the model parameters (S_{50} and D_0 only, see Section 5.3.3 for the treatment of outlying points when estimating g_{sx}). The number of points removed was less than 10 % of the total available at each of the ground-based sites.

Initial attempts at unconstrained optimisation of g_{sx}, S_{50} and D_0 using Equation 5.12 failed because Ω did not reach a minimum before one of the parameters reached an unrealistic, usually negative, value. This occurred for two reasons. First, the three quantities g_{sx}, S_{50} and D_0 are not independent and changing one forces a change in the other two. As an example, decreasing the value of D_0 increases the curvature of the modelled stomatal response to D but also decreases the magnitude of $f\left(D\right) = 1/\left(1 + D/D_0\right)$ for all non-zero values of D. The overall reduction in magnitude must then be balanced by either an increase in g_{sx} or a decrease in S_{50} if agreement between the observed and modelled G_c is to be preserved. Second, even after the outlying points have been removed, the observations of G_c, $S_\downarrow$ and D contain random errors. This means that the RMS difference can be reduced by either improving the overall fit of the model or by suppressing the model dependence on the variable associated with the empirical parameter being estimated. Unconstrained optimisation methods may drive the combination of parameters to unrealistic values in an attempt to remove the effect of random errors in the measurements on the RMS difference.

In order to constrain the solution, the initial value of g_{sx} for each site was chosen as $g_{sx} = 2.7G_{sx}$ where G_{sx} is the maximum observed surface conductance. Kelliher et al. (1995) found this relationship to be remarkably consistent over a large range of vegetation types and leaf area indices. A further advantage of this choice is that G_{sx} varies in response to soil moisture and setting $g_{sx} = 2.7G_{sx}$ allows soil moisture changes to be factored into g_{sx} and not into the estimates of S_{50} and D_0. The maximum surface conductance was chosen based on a histogram of the observed values rather than using the absolute maximum in order to guard against outlying points.

The optimisation was repeated with g_{sx} constrained to this initial value and resulted in a value of $0.005 \pm 0.003 \, \text{kg kg}^{-1}$ for D_0. The values for S_{50} were very scattered and no solution was found for the Wagga pasture, Cooinda canola and Urana pasture sites. The average of S_{50} estimates for the other sites was $60 \pm 70 \, \text{W m}^{-2}$. Attempts to improve the solution by iterating around values of g_{sx}, S_{50} and D_0 from successive optimisations failed to converge at all sites. These results indicate that there is no unique set of g_{sx}, S_{50} and D_0 values for the ground-based data and that the value of S_{50}, in particular, is poorly defined by the OASIS data.

Since there was no systematic dependence of S_{50} or D_0 on location along the transect or on land use, it was decided to use single values of these quantities for all sites. The values chosen were $100 \, \text{W m}^{-2}$ and $0.005 \, \text{kg kg}^{-1}$ for S_{50} and D_0 respectively. Kelliher et al. (1995) suggest a possible range of 25 to $100 \, \text{W m}^{-2}$ for S_{50}. Finkele et al. (2003), in a modelling study published after the work described here was performed, use a value of $0.015 \, \text{kg kg}^{-1}$ for D_0 and values of 150, 100 and $50 \, \text{W m}^{-2}$ for S_{50} at Wagga, Browning and Urana respectively. The optimisation process described above did not yield a robust estimate of g_{sx} for each site and an alternative method, described in the following section, was adopted.

5.3.3 Averaging Rules for Maximum Stomatal Conductance

The averaging scheme adopted here is a modification of those described in McNaughton (1994) and Raupach (1995) for calculating the average aerodynamic and surface conductance. The average g_{sx} is calculated from the average aerodynamic and surface conductances by inverting Equations 5.7 and 5.8. The constraints used by this scheme are that the resultant latent heat flux is equal to a linear average of the individual fluxes and that the form of the Penman-Monteith equation is preserved across scales. This choice means that the aerodynamic and surface conductances are calculated as weighted averages with the weights determined by the available energy and the saturation deficit. These "effective" values are not necessarily equal to the true averages and this may introduce error when they are used to calculate the average g_{sx}. Evidence that these errors are small is presented later in this section.

The averaging scheme is written in terms of resistances rather than conductances because this simplifies the algebra. Also, the radiative coupling between the available energy and the surface temperature is assumed to be small and is neglected (Raupach, 1995). This allows the aerodynamic resistances for heat and water vapour to be set equal to each other and further simplifies the final averaging scheme. The major difference between the scheme described here and those presented in McNaughton (1994) and Raupach (1995) lies in the treatment of the saturation deficit, the air density, and the change in latent heat content with change in sensible heat content. Their schemes consider a heterogeneous surface at an instant in time and this allows the approximation that all parts of the surface are exposed to the same values of these quantities. The modified scheme is intended for use throughout the diurnal cycle or over several days with different synoptic conditions and the approximation of constant D, ρ and ε can not be made. These quantities must now be carried through the averaging scheme resulting in a modest increase in complexity.

The Penman-Monteith equation can be written in terms of resistances as:

$$F_{E,i} = \frac{\varepsilon_i r_{a,i} F_{A,i} + \rho_i \lambda D_i}{r_{d,i}}$$

5.13

where $r_{a,i}$ is the aerodynamic resistance, $r_{d,i} = r_{a,i}(\varepsilon_i + 1) + r_{s,i}$ is the deficit resistance, $r_{s,i}$ is the surface resistance and the subscript i refers to a single observation. This may be a single aircraft pass or a single averaging period for ground-based measurements. An equivalent expression can be written for the average latent heat flux:

$$F_E = \frac{\varepsilon R_a F_A + \rho \lambda D}{R_d}$$

5.14

Following the convention used in Raupach (1995), capital letters are used to identify average surface properties, R_a and R_d, and lower case letters are used for quantities representing a single observation. The flux matching constraint requires that $F_E = \sum_i a_i F_{E,i}$ where $a_i = N^{-1}$ is the equal-weight accorded to each observation and N is the number of observations. Applying the flux matching constraint leads to:

$$\frac{\varepsilon R_a F_A + \rho \lambda D}{R_d} = \sum_i a_i \frac{\varepsilon_i r_{a,i} F_{A,i} + \rho_i \lambda D_i}{r_{d,i}}$$

$$\frac{\varepsilon R_a F_A}{R_d} + \frac{\rho \lambda D}{R_d} = \sum_i a_i \frac{\varepsilon_i r_{a,i} F_{A,i}}{r_{d,i}} + \sum_i a_i \frac{\rho_i \lambda D_i}{r_{d,i}}$$

5.15

Matching the first and second terms on the left and right hand sides of Equation 5.15 gives:

$$\frac{\varepsilon R_a F_A}{R_d} = \sum_i a_i \frac{\varepsilon_i r_{a,i} F_{A,i}}{r_{d,i}}$$

$$\frac{\rho \lambda D}{R_d} = \sum_i a_i \frac{\rho_i \lambda D_i}{r_{d,i}}$$

5.16

Rearranging Equation 5.16 gives expressions for the weighted average aerodynamic and deficit resistances:

$$R_a = \frac{R_d}{\varepsilon F_A} \sum_i a_i \frac{\varepsilon_i r_{a,i} F_{A,i}}{r_{d,i}}$$

$$R_d = \frac{\rho D}{\sum_i a_i \rho_i D_i / r_{d,i}}$$

5.17

The average surface conductance can then be calculated from R_a and R_d using:

$$G_s = \left(R_d - (\varepsilon + 1) R_a \right)^{-1}$$

5.18

The average maximum stomatal conductance is calculated using the inverse of Equations 5.7 and 5.8:

$$G_c = \frac{G_s \left(1 + G_a / \varepsilon G_i - \tau \right) - \tau G_a / (\varepsilon + 1)}{1 + G_a / \varepsilon G_i}$$

$$g_{sx} = \frac{c_Q G_c \left(1 + D / D_0 \right)}{\ln \left(\dfrac{S_\downarrow + S_{50}}{S_\downarrow \exp(-c_A L_{ai}) + S_{50}} \right)}$$

5.19

The value of G_a in Equation 5.19 is taken as $G_a = 1/R_a$ with R_a calculated using Equation 5.17. The required values of $S_\downarrow$ and F_A are calculated as linear averages of the individual observations. As Raupach (1995) points out, this is an approximation in the case of $S_\downarrow$, albeit a good one, that is only exact when there is no multiple scattering of the incoming radiation. The averages of ρ, ε and D are calculated after first averaging the temperature, pressure and specific humidity.

It was not necessary to remove the outlying points associated with anomalously large values of observed G_c when using the averaging scheme to estimate g_{sx}. This is because the averaging scheme weights the individual g_{sx} values by F_A and D. Most of the outlying points occur prior to 1100 when both F_A and D are small or in cloudy conditions, when F_A is small. The weighting reduces the impact of the outlying points on the average g_{sx} and means that the averaging scheme is a more robust method of estimating g_{sx} than the optimisation process described in Section 5.3.2.

The above scheme was checked by comparing F_E calculated as the average of the individual $F_{E,i}$ with F_E calculated using the average g_{sx} derived from Equations 5.17, 5.18 and 5.19. The F_E calculated using g_{sx} from the averaging scheme was 3% less than the averaged observations. The error is small and this means that the effective values of G_s and G_a can be used as surface properties without significant loss of accuracy.

5.3.4 Comparison of Observed and Modelled G_s

The comparison of the observed and modelled G_s is shown in Figure 5.1 for the crop and pasture sites at Wagga, Browning, Wattles, Cooinda and Urana. The values of g_{sx} from Table 5.1 in Section 5.4.3 were used to calculate the modelled G_s. The plots contain all available data for daylight hours, including outlying points.

The g_{sx} model agrees reasonably well with the observations for both the crop and pasture sites at Browning, Wattles, Cooinda and Urana. The model compares poorly with the observations at the Wagga crop site and shows no correlation with observations over the Wagga pasture site. Values of G_s at Browning are approximately half those at Wagga with a further halving between Browning and Urana. The reduction in G_s by a factor of four between Wagga and Urana reflects the drier conditions at the Urana end of the transect. Surface conductance values for the crops are higher than those for the pasture at both Browning and Urana since the crops have deeper roots and are able to draw on water from deeper in the soil column. The results show that, with the exception of the Wagga pasture site, the g_{sx} model reproduces the observed variation of G_s across the landscape and between land cover classes.

The poor performance of the g_{sx} model at the Wagga pasture site, Figure 5.1b, is due to imbalance in the terms of the surface energy budget. There is less correlation between $(F_N - F_G)$ and $(F_H + F_E)$ at this site ($r^2 = 0.74$) than at the other 7 sites ($r^2 \geq 0.9$) and the standard deviation of the difference between $(F_N - F_G)$ and

$(F_H + F_E)$ is greater, 63 W m^{-2} compared to $\leq$ 43 W m^{-2}. These results demonstrate a lack of equality between $(F_N - F_G)$ and $(F_H + F_E)$ from hour to hour, even though the budget is closed on average (Leuning et al., 2004), and this results in a large number of spurious values for the observed G_s calculated by inverting the Penman-Monteith equation. Expressing the available energy as $F_A = (F_H + F_E)$ raises the correlation between observed and modelled G_s from $r^2 = 0.0$ to $r^2 = 0.55$ at this site with smaller improvements for the other sites.

The outlying points in Figure 5.1 are associated periods when the surface energy budget does not close, during non-stationary conditions or when the canopy was wet after rain or dew fall. These points were manually removed on the basis of objective criteria before the estimation of S_{50} and D_0 but were included in the estimation of g_{sx}. This is because the averaging scheme used to estimate g_{sx} weights the individual g_{sx} values by F_A and D, both of which tend to be small for the outlying points. This makes the averaging scheme robust compared to the optimisation method used to estimate S_{50} and D_0. The outlying points are included in the comparison plots to indicate the spread of available data.
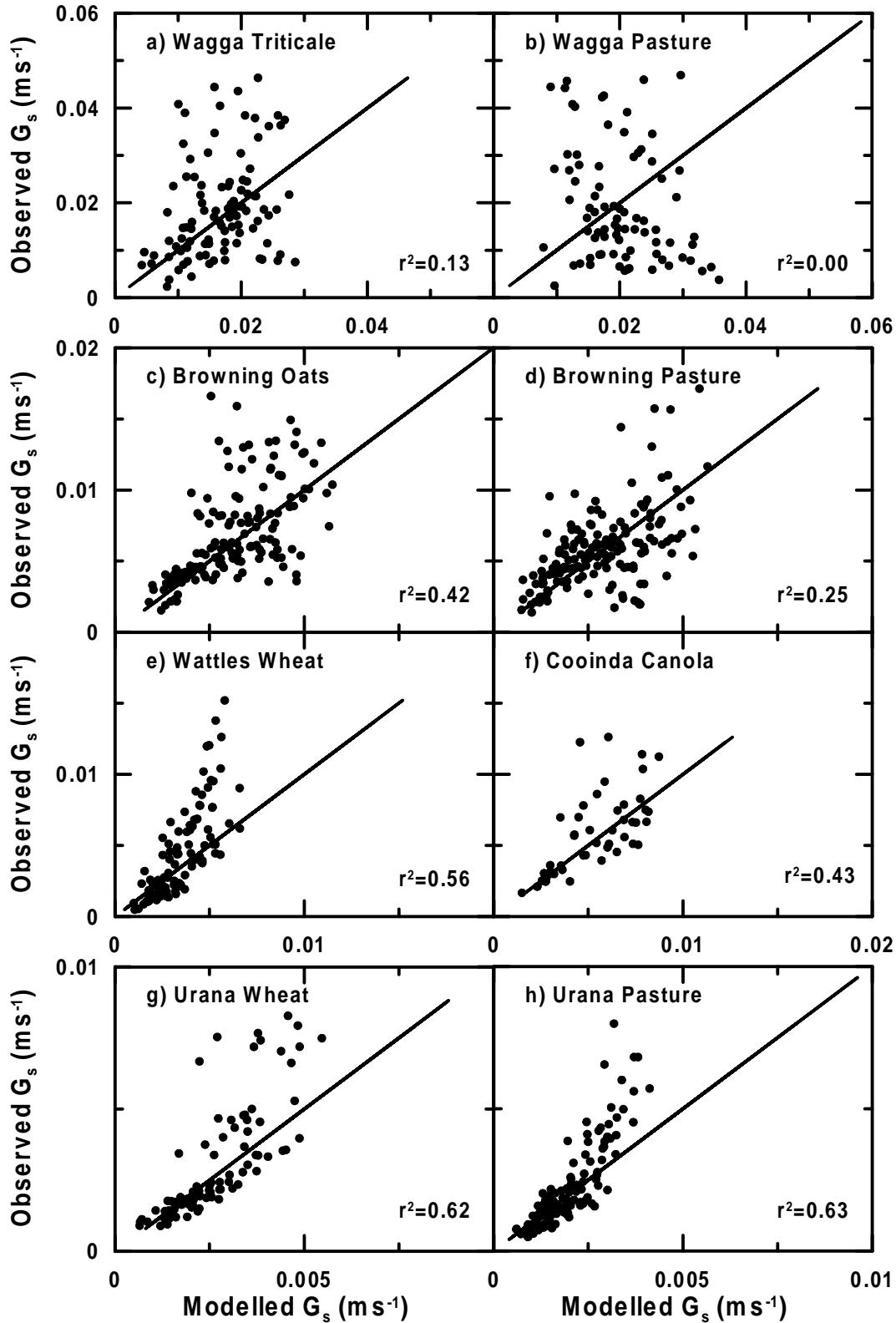
Figure 5.1 Comparison of observed and modelled G_s for the crop and pasture sites at Wagga a) and b), Browning c) and d), Wattles e), Cooinda f) and Urana g) and h). Solid line is 1:1.
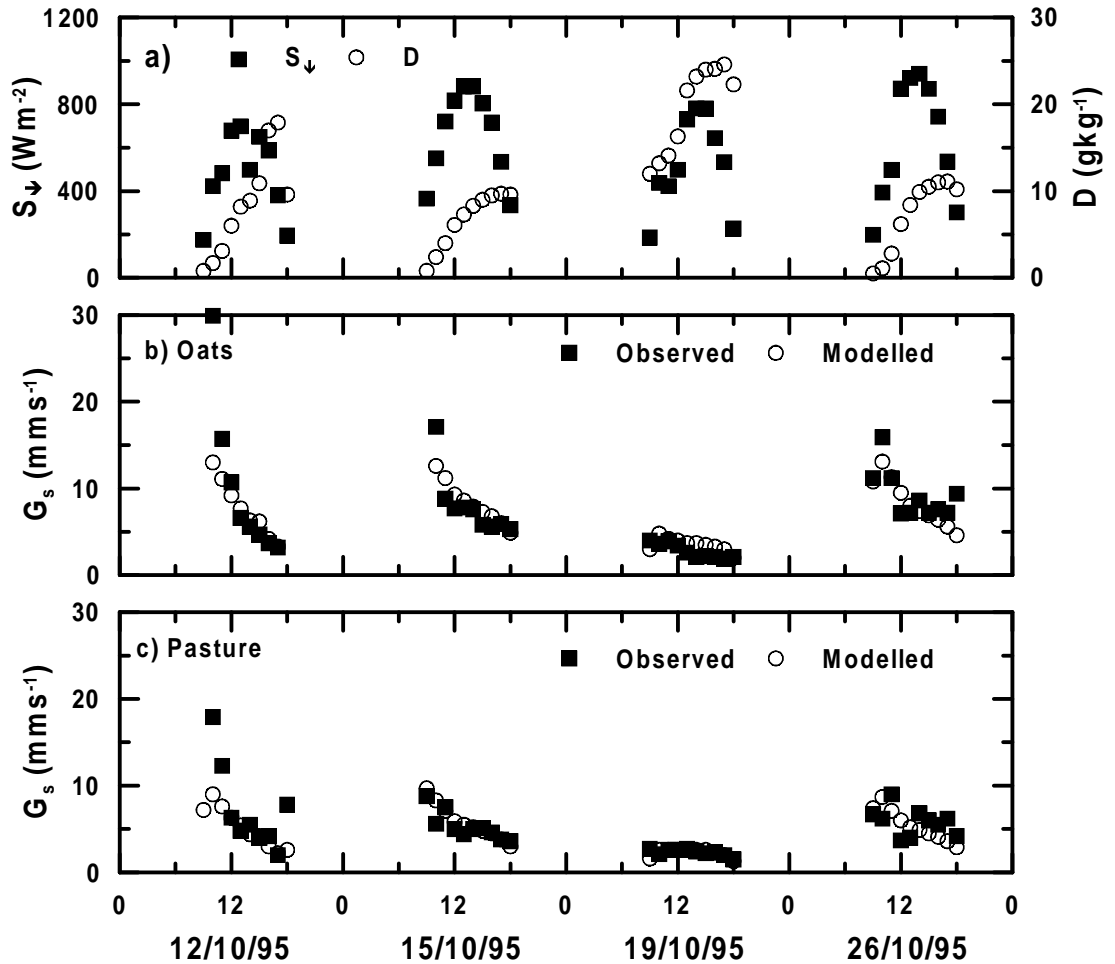
Figure 5.2 Diurnal variation of a) $S_\downarrow$ and D and b), c) G_s from the inverted Penman-Monteith equation (Observed) and the g_{sx} model (Modelled) for four days at the Browning crop and pasture sites.

The diurnal variation in $S_\downarrow$, D and G_s is plotted in Figure 5.2 for four days of ground based measurements at the Browning crop and pasture sites. Observed values of G_s were calculated by inverting Equation 5.5 and the modelled values were calculated using Equations 5.7 and 5.8. The modelled G_s agrees well with the ground based observations and reproduces most of the diurnal and day to day trends. The largest differences are seen between 0800 and 1000 on mornings where the saturation deficit had dropped to zero just before dawn, as happened on 12, 15 and 26 October 1995. Values of D close to zero suggest dew fall occurred overnight and that the large values of observed G_s at these times are associated with evaporating dew, a process not represented in the model for surface conductance.

5.4   Results

5.4.1   General

The criteria for surface properties to be useful in predicting regional scale fluxes were presented in Section 5.1.1. This section assesses α_E, β, g_{sx} and W_{UE} against these criteria by examining the diurnal, daily and spatial variability in the surface properties.   The site-to-site variability, for example between adjacent crop and pasture sites, determines the ability of a surface property to discriminate between different land uses and hence the extent to which values for the surface property can be assigned on the basis of vegetation class. A small or non-existent diurnal trend allows the value of a surface property to be estimated from limited number of observations during part of the day. Variation in the daily value of a surface property is undesirable because it indicates that the surface property is sensitive to synoptic conditions.   Spatial variability in a surface property is desirable because it demonstrates the ability of the surface property to resolve surface heterogeneity.

5.4.2   Closure of Surface Energy Budget

The closure of the surface energy budget can be expressed in terms of the ratio of the sum of the turbulent fluxes to the available energy:

$$m_{SEB,i} = \left(F_{H,i} + F_{E,i} \right) \Big/ \left(F_{N,i} - F_{G,i} \right)$$

$$\bar{m}_{SEB} = \sum_{i=1}^{I} \left(F_{H,i} + F_{E,i} \right) \Big/ \sum_{i=1}^{I} \left(F_{N,i} - F_{G,i} \right)$$

5.20

where $F_{N,i}$, $F_{G,i}$, $F_{H,i}$ and $F_{E,i}$ are the individual observations of net radiation, ground heat flux, sensible heat flux and latent heat flux respectively, $m_{SEB,i}$ is the ratio for each individual observation of the surface energy budget and $\bar{m}_{SEB}$ is the average ratio over all I observations in the data set. Note that obtaining F_H and F_E from the temperature and humidity gradients using the Bowen ratio technique forces $\bar{m}_{SEB} = m_{SEB,i} = 1$ and hides the effects of the lack of closure from the researcher.

Finnigan (2004) and Finnigan et. al. (2003) give an exhaustive discussion of some of the possible reasons for non-closure of the surface energy budget.

Lack of closure for the surface energy budget is indicated by non-unity values of the ratio and influences the values of α_E and g_{sx} estimated from the ground-based and aircraft data. The evaporative fraction is affected by virtue of its definition as the ratio of F_E and $F_A = F_N - F_G$ (Equation 5.1). The maximum stomatal conductance is affected through its dependence on G_s (Equations 5.10 and 5.11) which is in turn dependent on the ratio of F_E and $F_A = F_N - F_G$ (Equation 5.9).

$m_{SEB,i}$ varies about 1 for the OASIS data set and this causes random error in the observed values of α_E and g_{sx}. By contrast, $\bar{m}_{SEB}$ is most often less than 1 for daylight hours in the OASIS data set causing a systematic error in α_E and g_{sx} proportional the departure of $\bar{m}_{SEB}$ from unity. This is of particular concern when data from ground-based and airborne systems, are being compared because differences in $\bar{m}_{SEB}$ between the data sets will give rise to systematic errors in α_E and g_{sx} of different sizes. For example, the value of $\bar{m}_{SEB}$ varies from 0.827 to 0.990 for data from the ground-based sites and from 0.94 to 1.08 for the aircraft data. To avoid systematic errors of different magnitudes for each data set, the ground-based and aircraft observations of F_H and F_E have been scaled as follows:

$$
\begin{aligned}
F'_{H,i} &= F_{H,i} / \bar{m}_{SEB} \\
F'_{E,i} &= F_{E,i} / \bar{m}_{SEB}
\end{aligned}
\qquad 5.21
$$

where $F'_{H,i}$ and $F'_{E,i}$ are the corrected values used to calculate the observed α_E and g_{sx}. The correction is equivalent to assuming that the lack of closure is due to systematic errors in the turbulent fluxes and that the errors are the same for F_H and F_E, i.e. that the measured Bowen ratio is correct (Cleugh et. al., 2004).

The maximum changes between using the scaled and non-scaled values of F_H and F_E are 35 % for g_{sx} derived from the ground-based data at the Wagga crop site and 16 % for g_{sx} derived from the aircraft data at Wagga. Differences between α_E and

g_{sx} values calculated using scaled and non-scaled F_H and F_E at all other sites did not exceed 10 %. The mean difference between the observed and modelled F_E (see Chapter 7) decreases by 5 % when α_E and g_{sx} are calculated using the scaled values of F_H and F_E.

5.4.3 Surface Properties at Ground-based Sites

Table 5.1 lists the average values for the surface properties at the ground-based sites during the 1995 OASIS experiment, calculated using the methods described in Sections 5.2.2 and 5.3.3. All of the surface properties show a strong trend from Wagga to Urana in response to the rainfall gradient and consequent soil moisture variation but only W_{UE} shows a consistent difference between crop and pasture sites. This is in agreement with the results of Kelliher et al. (1995) who also found no systematic difference in g_{sx} between crops and pasture. The results indicate that at any given location along the transect the crop and pasture fields lose similar amounts of water but the crops gain significantly more carbon in return. Values for the surface properties at the Wattles site are similar to those for the Urana crop and pasture sites and this suggests that the wheat crop at Wattles was transpiring less water than the adjacent crops and pasture at Browning and Cooinda.

Table 5.1 Values of α_E, g_{sx}, β and W_{UE} for the ground-based sites during the 1995 OASIS experiment.

		α_E	g_{sx} mm s^{-1}	β	W_{UE} mgCO$_2$ gH$_2$O
Wagga	Triticale	0.79	14.0	0.27	-9.05
	Pasture	0.77	21.2	0.30	-7.42
Browning	Oats	0.56	5.9	0.80	-6.07
	Pasture	0.59	6.1	0.70	-1.86
Wattles	Wheat	0.41	3.3	1.44	
Cooinda	Canola	0.57	5.8	0.77	
Urana	Wheat	0.37	2.4	1.73	
	Pasture	0.38	1.2	1.62	

5.4.4   Diurnal Variation of α_E, g_{sx}, β and W_{UE}

Figure 5.3 shows the diurnal variation in F_A, F_E, F_C, α_E, g_{sx}, β and W_{UE} for four days of ground based measurements at the Browning site. The available energy and the latent heat flux vary by an order of magnitude through the course of the day, increasing from a few tens of W m^{-2} in the morning to a few hundreds of W m^{-2} at the midday peak and decreasing again in the late afternoon. The variation in the surface properties is much less. The diurnal trend in α_E and g_{sx} is typically less than 50% with the exception of some outlying points before 0900 and after 1500 local time. These are associated with the evaporation of dew and the maintenance of evapotranspiration by downward sensible heat flux (Oke, 1987) respectively. The Bowen ratio and W_{UE} both show significant variation during the day and from day to day, especially for the crop site where W_{UE} tends to have a large magnitude in the morning and decreases through to early afternoon.
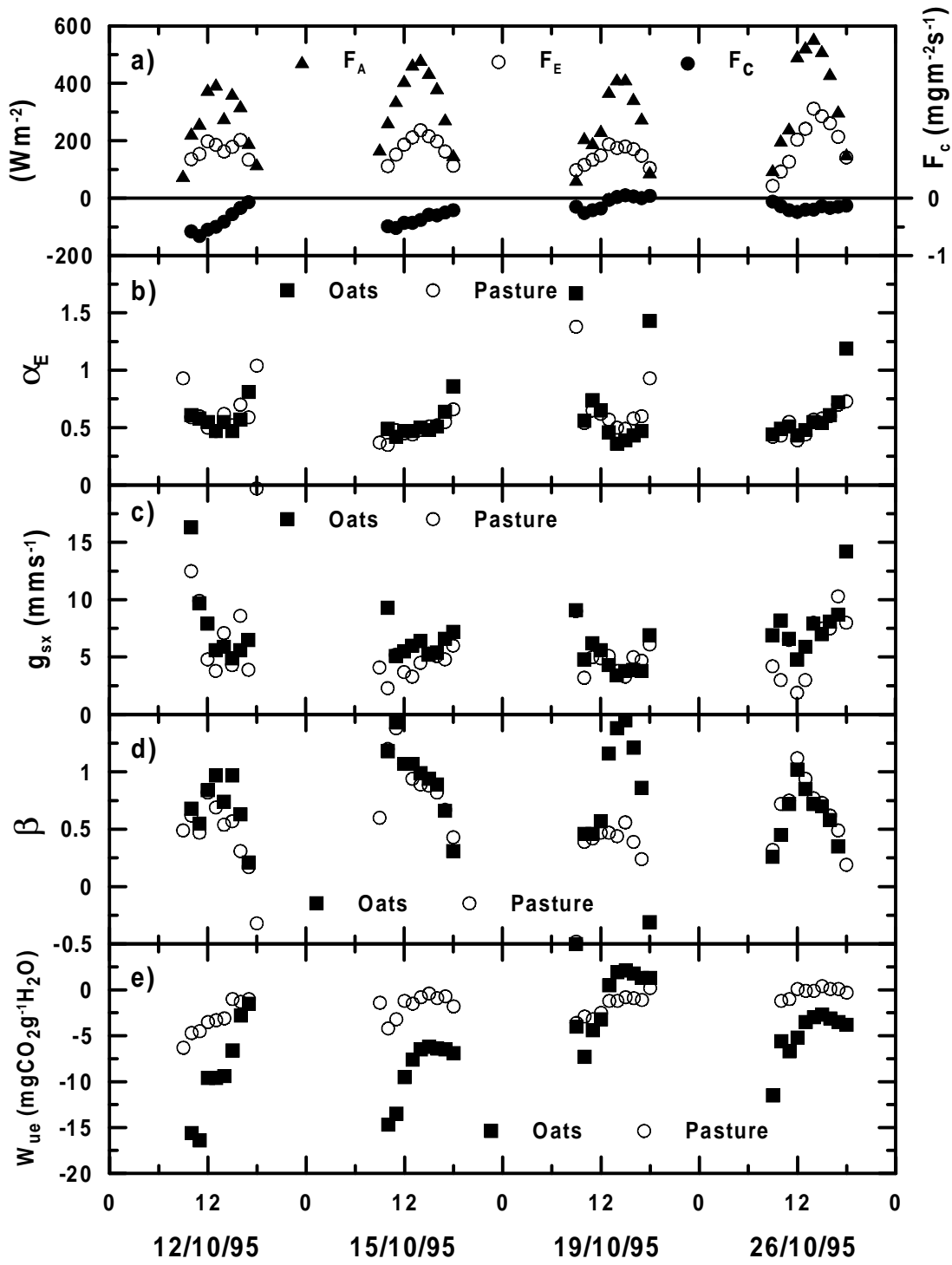
Figure 5.3 Diurnal variation of a) F_A, F_E and F_C, b) α_E, c) g_{sx}, d) β and e) W_{UE} for four days at the Browning crop and pasture sites.
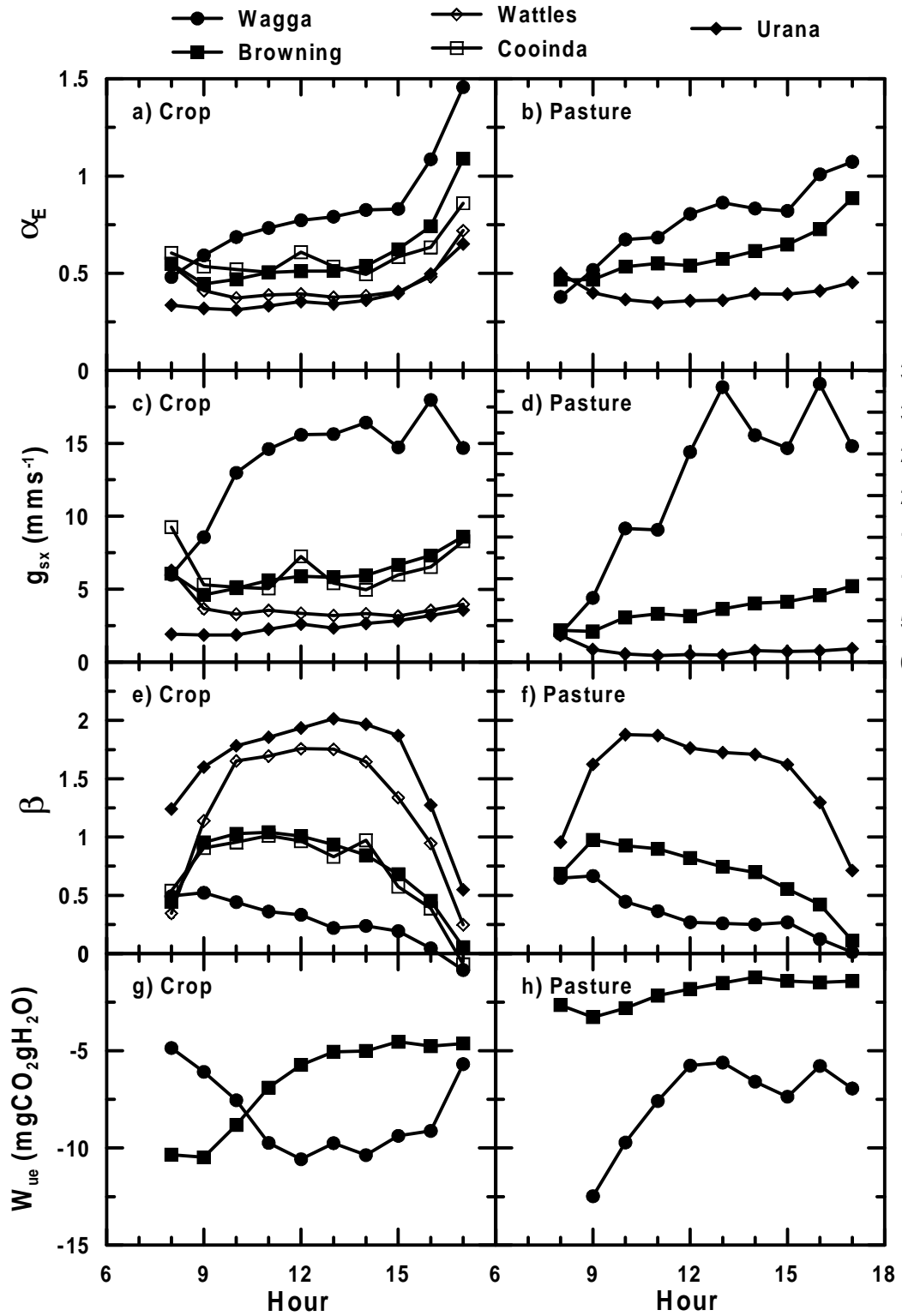
Figure 5.4 Diurnal variation of α_E, g_{sx}, β and W_{UE} for all available days at the crop (a, c, e, g) and pasture (b, d, f, h) sites. Note the different scales on the g_{sx} plots.

The diurnal variation in α_E, g_{sx}, β and W_{UE} for the ground based sites averaged over all available days is shown in Figure 5.4. α_E and g_{sx} remained within 10% of their midday values for about six hours (1000 to 1500 inclusive) at the Wagga crop site and the crop and pasture sites at Browning, Wattles, Cooinda and Urana. The Bowen ratio, β, shows a pronounced diurnal variation with small values in the morning and evening and broad peak around midday. The diurnal course of W_{UE} at Wagga pasture and Browning crop shows a general decrease in magnitude from morning to afternoon. When data from the paired crop and pasture sites are averaged, W_{UE} remains within 10% of the midday value for five hours (1000 to 1400 inclusive) at Wagga and Browning. Although α_E, g_{sx} and W_{UE} are not constant throughout the day, they show significantly less diurnal variation than the fluxes themselves. Most aircraft flights during OASIS occurred between 1100 and 1500 when variation in the surface properties was small. The results demonstrate that α_E, g_{sx} and W_{UE} at a given location can be estimated with reasonable accuracy from aircraft flights during the middle part of the day.

5.4.5   Daily Variation of α_E, g_{sx}, β and W_{UE}

This section investigates the sensitivity of the surface properties to synoptic conditions by examining their daily variation. Surface properties are expected to change at seasonal scales in response to climatic forcing but variation at daily scales is interpreted as evidence of sensitivity to synoptic conditions. The sensitivity may be real or due to deficiency in the model used to infer the surface property from observations.

Figure 5.5 shows time series plots of daily values for α_E, g_{sx}, β and W_{UE} derived from the ground-based and aircraft data at Wagga, Browning and Urana. Each row in Figure 5.5 corresponds to a particular surface property and each column corresponds to a location along the transect from Wagga to Urana. Arrows adjacent to the date axis indicate days on which rain fell. The amounts during the two periods were 6.4, 8.4 and 7.4 mm (13 October) and 34.8, 48.8 and 43.0 mm (21-22 October) for Wagga, Lockhart and Urana respectively.

The results confirm the west to east gradient in the surface properties shown in Table 5.1. There is also a general trend at each site in response to the draw down of soil moisture during the 19-day experiment period. This is most evident in α_E, β and W_{UE}. All of the surface properties show significant day to day variation in response to changing synoptic conditions but the nature of the response varies with location along the transect. At Wagga, the surface properties show the largest change in response to advective conditions on 17, 19 and 20 October 1995 when evapotranspiration was driven by both F_A and F_H, leading to values of α_E greater than one and large values of g_{sx}. This response is only possible if the soil moisture level is high enough to support the large water loss by the surface in these conditions. At Browning and Urana, the surface properties show the largest change in response to rainfall events when the soil water store was briefly recharged. This suggests that soil moisture was limiting plant growth at these sites.

The results show that all of the surface properties are sensitive to changes in meteorology and soil moisture at both synoptic (on the order of days) and seasonal (on the order of weeks) time scales. This is understandable in the case of the simple ratios, α_E, β and W_{UE}, because these include no mechanism to explain plant response to changing meteorological conditions. The day to day change in g_{sx} occurs because the model used to infer g_{sx} from the observations fails in advective conditions when $F_A \neq F_H + F_E$ and it does not include a soil moisture term. In general, the day to day variability in the surface properties is of similar magnitude to the site to site differences and this means that data from several days must be averaged to reduce the random error in the surface property estimates.
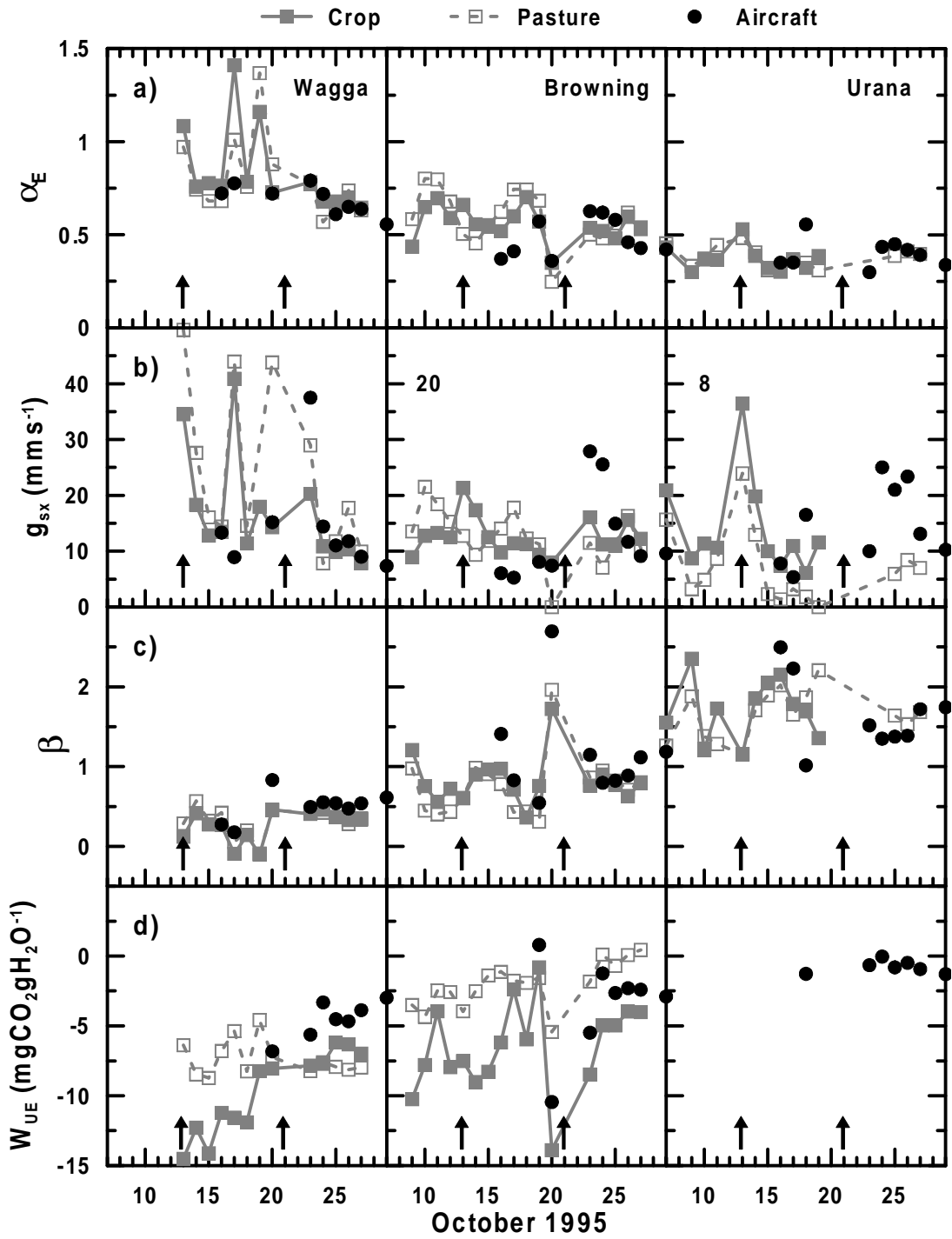
Figure 5.5   Daily values for a) α_E, b) g_{sx}, c) β and d) W_{UE} at Wagga, Browning and Urana. Arrows indicate days when rain fell. Note the use of different scales in the g_{sx} plots.

5.4.6 Spatial Variability of α_E, g_{sx}, β and W_{ue}

Figure 5.6 shows the spatial variability of α_E, g_{sx}, β and W_{UE} over the 10 km by 10 km grid area near Lockhart. The data come from six grid flights at 20 mAGL that were flown on 23 to 29 October 1995. Data from the six flights have been averaged as described in Sections 5.2.2 and 5.3.3.

All four surface properties show similar patterns, with low (α_E, g_{sx}) or high (β, W_{UE}) values in the NW and SE corners and a central band of higher (or lower depending on the quantity) values running from NE to SW. These patterns are consistent with the underlying terrain, with higher (or lower) values occurring over the shallow depression that runs NE to SW east across the bottom half of the grid area. The general picture is of a more active surface, greater transpiration and assimilation, within this shallow depression and a less active surface on the higher ground to the north and south.

Figure 5.7 shows the variability of the composite surface properties along the transect. The aircraft data come from flights on 11 days from 16 to 29 October 1995 at between 20 and 30 mAGL. The ground-based data come from all available days of measurements. There is good agreement between the surface properties estimated using the aircraft and ground-based data at Browning and Urana. The ground-based values for Wagga are higher (α_E, g_{sx}) or lower (β, W_{UE}) than the aircraft data, especially for g_{sx} at the Wagga pasture site. This suggests that the Wagga crop and pasture sites may not have been representative of the adjacent surface sampled by the aircraft.
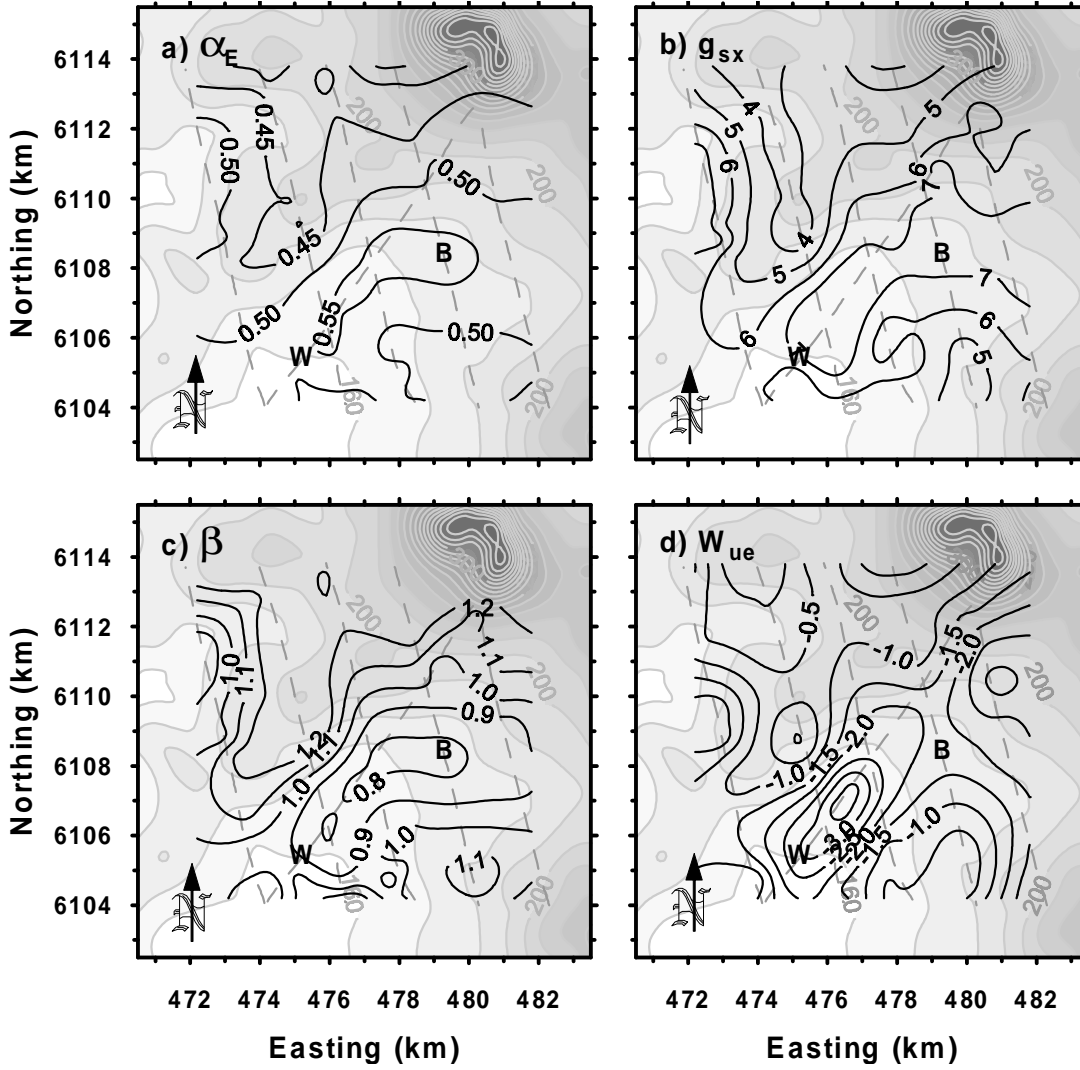
Figure 5.6 Contour maps of a) α_E, b) g_{sx}, c) β and d) W_{UE} over the grid area near Lockhart. The dotted grey line is the aircraft flight track. Terrain contours are at 10 m intervals and the terrain shading darkens with height.
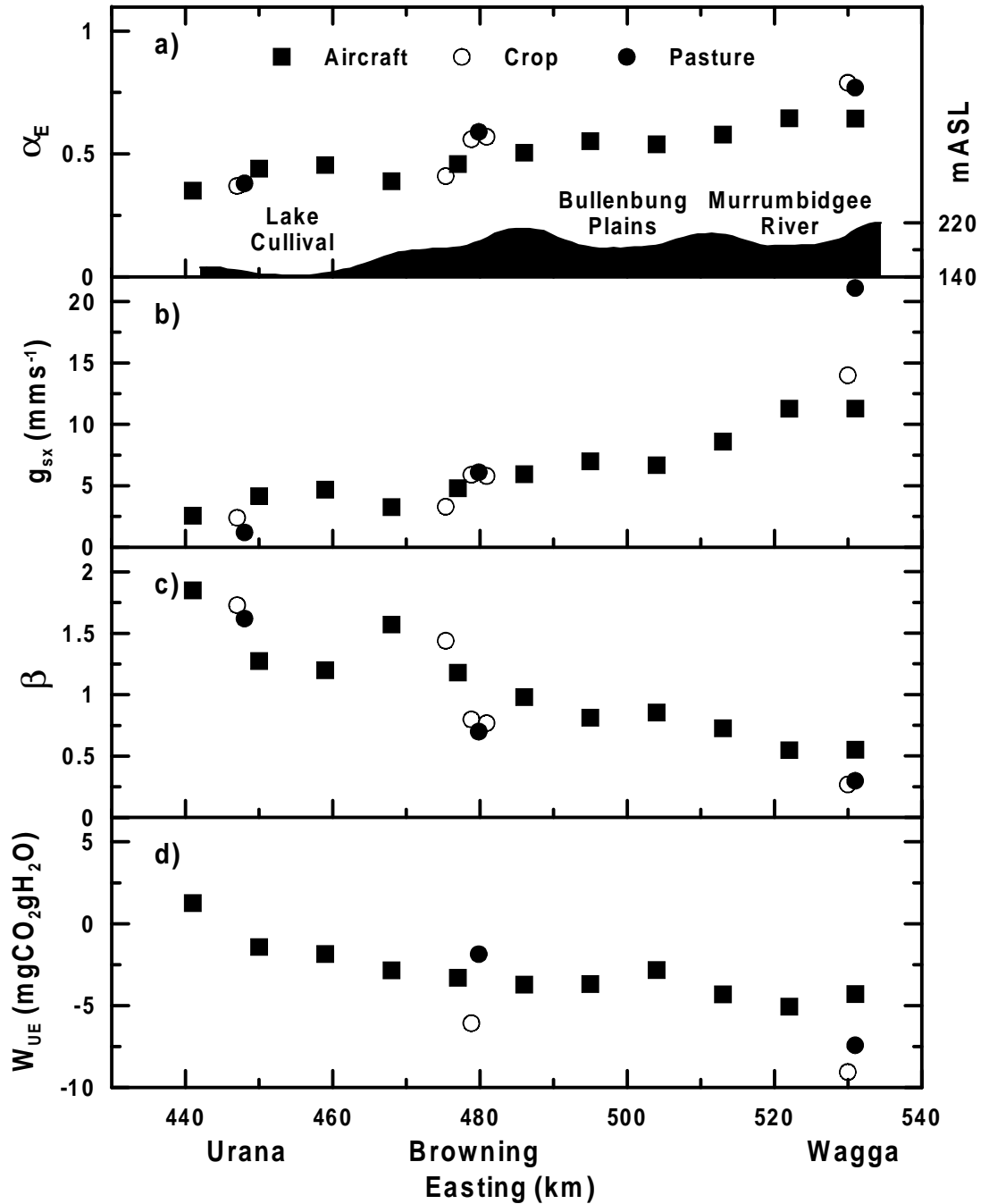
Figure 5.7 Variation of a) α_E, b) g_{sx}, c) β and d) W_{UE} estimated from aircraft and ground based data along the transect. Values for the crop and pasture fields at each ground-based site are plotted as open and filled circles respectively, aircraft data are plotted as filled squares.

All of the surface properties show a strong trend from east to west in response to the rainfall gradient. Fluctuations about the trend are also similar, especially around the Murrumbidgee River, the Bullenbung Plains and Lake Cullival. The most likely explanation for the local deviations from the overall trend is changes in soil moisture

due to rain-shadows in the lee of the ridge at the western edge of the Bullenbung Plains and local drainage patterns around Lake Cullival.

These results show that the surface properties clearly resolve the heterogeneity found across the OASIS experimental domain at two spatial scales. The grid data reveals significant heterogeneity in a 10 km by 10 km area of uniform land use that is consistent with the underlying terrain and the expected effect of local drainage patterns. The transect data shows heterogeneity at scales of 10 km and 100 km and reveals detail not sampled by the network of ground-based sites. The observed heterogeneity is again consistent with the underlying terrain and its effect on soil moisture. At the 100 km scale, the change in the surface properties appears to be driven by variations in the soil moisture due to the large-scale rainfall gradient. At the 10 km scale, the surface heterogeneity appears to be forced by local microclimate and drainage patterns, again through the modulation of soil moisture.

5.5 Summary and Conclusions

Aircraft data provide good spatial but poor temporal estimates of the surface fluxes of heat, water vapour and carbon dioxide, whereas ground based data provides poor spatial but good temporal information. The two sources of data can be combined to take advantage of these complementary strengths via parameters that are more descriptive of the surface than the fluxes themselves. Four such surface properties have been examined here. Three of these are simple ratios of fluxes, the evaporative fraction $\alpha_E = F_E/F_A$, the Bowen ratio $\beta = F_H/F_E$ and the water-use efficiency $W_{UE} = \lambda F_C/F_E$.

The fourth surface property, g_{sx}, is defined as the maximum stomatal conductance achievable by leaves at the top of a vegetation canopy under optimal conditions. Optimal conditions require that plant function is not limited by soil water availability and Leuning et al. (2004) show that this situation only occurred at Wagga during the 1995 OASIS experiment. As a consequence, the values of g_{sx} calculated for Browning and Urana are smaller than those quoted by Kelliher et al. (1995) and vary by location in response to soil moisture. The empirical parameters, S_{50} and D_0, proved difficult to estimate from the ground-based data due to the limitations of this model of stomatal function. In particular, the dependence of canopy conductance on light was derived in Kelliher et al. (1995) by considering the response of stomata to light as it attenuates with increasing depth in a canopy and the resulting model predicts that G_c is monotonic with $S_\downarrow$. However, the data show that G_c varies from high values in the morning to low values in the afternoon as the stomata respond to an increasing saturation deficit and the depletion of soil moisture in the root zone (Tuzet et al., 2003). This means that the same value of $S_\downarrow$ occurring in the morning or in the afternoon will be associated with different values of G_c. This obscures the relationship between G_c and $S_\downarrow$, making S_{50} difficult to determine. D_0 is better defined by the observations but the mutual dependence of g_{sx}, S_{50} and D_0 makes determination of a unique value impossible. The solution adopted here was to

constrain g_{sx} and S_{50} in order to estimate D_0 and then to use the same values of S_{50} and D_0 at all sites to calculate g_{sx} using an averaging scheme based on the linear averaging of F_E.

The diurnal trend in α_E and g_{sx} is small between the hours of 1100 and 1500 and this allows the daily value of these quantities to be estimated from aircraft data collected during this period. The results are less clear for W_{UE} but data averaged between paired crop and pasture sites suggests the magnitude of W_{UE} remains close to the daily average throughout the late morning and early afternoon. This means that data collected during this period may be used to predict the average value of W_{UE} but not its daily evolution. The diurnal trend in β is too large for it to be a useful approach to estimating regional scale fluxes.

The day-to-day variability in the surface properties due to random errors in the measurements and changing synoptic conditions is similar to the spatial variability observed across the OASIS domain. This means that the surface heterogeneity may not be accurately captured by measurements of α_E, β, W_{UE} and g_{sx} on a single day and it will usually be necessary to average the data from several days in order to obtain representative values. Averages of α_E, β and W_{UE} were obtained by averaging the component fluxes and an extension of the scheme proposed by McNaughton (1994) and Raupach (1995) was developed to calculate an average value for g_{sx}. Good agreement was found between F_E modelled using the average g_{sx} and the observed F_E.

The averaged surface properties derived from the ground-based and aircraft data show strong west to east changes along the transect that are driven by the rainfall gradient and the consequent gradient in soil moisture. In general, the differences in the surface properties between crop and pasture are small compared to the site-to-site variation. This prompts the conclusion that soil moisture plays a larger role in determining the fluxes of water vapour and CO_2 than the different land-uses encountered during the 1995 OASIS experiment. This result confirms that a

patchwork surface of crop and pasture can be modelled as a single surface type provided variations in soil moisture are accurately resolved.

The surface properties α_E, β, g_{sx} and W_{UE} are useful descriptions of surface heterogeneity when they can be averaged over several days but the variation of β during the day is too large for prediction of regional scale fluxes from a single value. The diurnal variation in α_E and g_{sx} is small enough to allow both daily average fluxes and the diurnal evolution of the fluxes of water vapour to be predicted from a single daytime value. The diurnal trend in W_{UE} is not well defined by the results of this study but a constant value recorded in the middle part of the day may be used to predict the daily average flux of CO_2, though not its diurnal evolution. The aircraft results reveal spatial variability in the surface properties at scales of 10 km and less that is not sampled by the ground-based network and may play a significant role in determining the regional scale fluxes. This makes it attractive to find a method for interpolating the surface properties over a much wider area than that covered by the ground-based network and the aircraft flights. The relationship between the surface properties and a remotely sensed quantity, the Normalised Difference Vegetation Index ($NDVI$), is examined in the next chapter as a possible basis for this interpolation.